Edelweiss Applied Science and Technology
ISSN: 2576-8484
Vol. 8, No. 6, 2789-2808
2024
Publisher: Learning Gate
DOI: 10.55214/25768484.v8i6.2558

Optimization of coupling phase-change materials and thermal screens in façade-integrated hybrid photovoltaic collectors for optimal energy production and thermal comfort in buildings

Kokou Aménuvéla Toka[1*], Yawovi Nougblégа[1,2], Yemboate Doubik Laré[1], Kodjo Kpodé[3]
[1]Laboratoire Sur l'Energie Solaire /Groupe Phénomènes de Transfert et Energétique, Université de Lomé, 01 Lomé BP 1515, Togo; tokakokou@gmail.com (K.A.T.) laredoubik@gmail.com (Y.D.L.).
[2]Regional Centre of Excellence on Electricity Management (CERME), University of Lomé, Togo; nycogl@yahoo.fr (Y.N.).
[3]Laboratoire de Matériaux, Energie Renouvelable et Environnement de l'Université de Kara, Togo; k.kpode@univkara.net (K.K.).

Abstract: The operation of building-integrated photovoltaic (BIPV) systems gives rise to a significant proportion of the solar radiation absorbed by the cells being unable to be converted into electricity. This phenomenon consequently increases the temperature. This temperature increase impacts the cells' electrical efficiency, leading to a reduction in their performance and accelerating their degradation. The combination of phase-change materials with insulating fluid blades, situated behind photovoltaic cells, represents a passive cooling solution that optimizes the performance of hybrid photovoltaic systems when incorporated into facades. The present study assesses a system that incorporates paraffin as a PCM and an argon layer in a PV-PCM-argon layer physical model (PVT/ArPCM), in comparison with a PV-PCM system (PVT/PCM), to enhance the thermoelectric performance of photovoltaic systems mounted on façades while ensuring optimal thermal comfort within buildings. The discrete heat transfer equations were solved using the Thomas algorithm and the iterative Gauss-Seidel method in conjunction with the implicit finite difference method. The findings illustrate that the electrical efficiency experienced only a slight increase, estimated at 0.01%, while there was a notable enhancement in the indoor thermal comfort experienced by occupants, with a 65% improvement observed due to the incorporation of an argon-filled thermal screen. The incorporation of an argon layer led to a minor reduction in temperature of 0.01°C in the photovoltaic cells, resulting in a minimal improvement of 0.014% in electrical power production. The phase-changing material incorporated into PVT/ArPCM demonstrated superior thermal management capabilities in comparison to the same material employed in PVT/PCM.

Keywords: *Argon layer, Heat transfer, Numerical study, Phase change materials, Photovoltaic coating.*

1. Introduction

It is estimated that buildings account for over 40% of global energy consumption [1], [2]. It is thus apparent that enhancing the energy efficiency of this sector constitutes a key response to the issue of energy shortages. In climates where high temperatures prevail, the majority of the energy consumed is allocated to the provision of air conditioning, encompassing both cooling and dehumidification. In tropical climates, heating, ventilation, and air conditioning (HVAC) systems can account for over 50% of a building's energy consumption, due to the high demand for cooling technologies to eliminate thermal loads [3]. This evidence highlights a significant opportunity to improve the energy efficiency of air conditioning systems. The fundamental principles of bioclimatic building design encompass a range of techniques aimed at reducing heat gain by limiting the exposure of building envelopes to solar radiation.

* Correspondence: tokakokou@gmail.com

Among the various techniques available for achieving energy efficiency, the utilization of thermal insulation materials on building walls is of particular importance [4]. The integration of insulating materials is a critical component of energy-efficient construction, as it facilitates the reduction of heating and air conditioning consumption while simultaneously enhancing indoor thermal comfort. The selection of an optimal insulation material is contingent upon several factors, including its thermal conductivity, cost, fire resistance, and environmental impact. In Europe, fire-resistant mineral wools (composed of glass and rock) represent 58% of the market, while flammable plastic foams (such as polyisocyanurate, expanded polystyrene, extruded polystyrene, and polyurethane) account for the remaining 41%. While the global market for materials such as aerogels and vacuum insulation panels demonstrates growth, the high cost and installation challenges associated with these products restrict their implementation on a larger scale [5]. Notwithstanding the technical difficulties inherent in the system, such as heat loss at the junctions, vacuum glazing is being investigated for use in conjunction with technologies such as photovoltaic glass. The system is designed to optimize thermal insulation, minimize solar heat gain, and promote energy self-sufficiency in buildings. One study indicates that this technology performs particularly well in cold climates, with an annual energy consumption reduction of 76.3%. In hot climates, the reduction in energy consumption was 59.4%. Despite the technical challenges associated with heat loss at joints, the potential of vacuum glazing is being investigated in conjunction with other technologies, such as photovoltaic glass. The system optimizes thermal insulation, thereby reducing solar heat gain and promoting energy self-sufficiency in buildings. It has been demonstrated in a study that this approach is notably efficacious in cold climates, with an annual reduction in energy consumption of 76.3%. In hot climates, the figure declines to 59.4%. The incorporation of photovoltaic components on building facades represents an active solution that can enhance thermal performance while simultaneously generating energy from renewable sources [6]. This process allows for the optimization of the building envelope, facilitating the capture of urban solar energy. However, in dry, hot climates, the temperature of photovoltaic cells frequently exceeds the recommended limits (40 to 85°C), thereby reducing their efficiency and durability. It is therefore imperative that their temperature be regulated [7], [8]. To this end, advanced thermal management strategies have been developed to optimize electrical efficiency while reducing the degradation of photovoltaic modules. In a study conducted by Nougbléga et al. [9] the thermal and electrical performance of hybrid collectors equipped with thermal screens was examined. The results demonstrated that a PVT hybrid collector operating within a vacuum environment exhibited enhanced thermal efficiency in comparison to a PVT hybrid collector with a constrained air gap. Nevertheless, the latter collector exhibits superior electrical efficiency.

The incorporation of an air gap situated behind the photovoltaic panels, to limit the transfer of heat through the walls, has been demonstrated to be an ineffective solution, subsequently reducing the appeal of these air-based systems [10]. The presence of air within the pores or cells of a material hinders the transfer of heat by convection; this is due to the high viscous drag exerted on the cell walls. To further reduce heat transfer, it is possible to replace the air with a low-conductivity gas, such as argon [11]. In a related study, Antonanzas et al. [12] investigated the potential of argon and xenon as substitutes for air in photovoltaic systems. Their findings demonstrated that these gases can enhance system performance under a range of operational conditions. However, it seems that argon is the optimal choice in terms of cost and environmental impact. Irshad et al. [13] employed modelling techniques to assess the performance of a Trombe wall equipped with photovoltaic elements, evaluating it with three types of glazing: single glazing, double glazing, and argon-filled double glazing. The findings indicate that argon-filled double glazing has a significant impact on reducing the cooling load, while also boosting the generation of electrical energy. Consequently, the studies provide substantiation for the economic and ecological significance of argon-filled double glazing, particularly in hot climates, to energy savings and reduced CO_2 emissions.

In recent years, some research teams have discussed the potential applications of phase-change material (PCM) systems in photovoltaic (PV) modules, noting their efficacy in efficiently cooling PV

Edelweiss Applied Science and Technology
ISSN: 2576-8484
Vol. 8, No. 6: 2789-2808, 2024
DOI: 10.55214/25768484.v8i6.2558

cells or modules [14]. One advantage of PCM-based cooling over that provided by natural air convection is that the capacity of the former to absorb heat without significant temperature variation is a relatively simple phenomenon. A phase-change material (PCM) is capable of absorbing or releasing thermal energy during a physical phase transition, thereby maintaining a minimal temperature change throughout the process. There are several methods by which solar photovoltaic systems can be integrated with phase change materials (PCM). The simplest method is to affix containers containing a phase-change material to the rear face of the solar panel [15]. The transfer of surplus thermal energy from the solar cells to the phase-change material enables its conversion into latent heat, thus contributing to the overall energy balance. The utilization of materials designed to absorb the excess heat produced by photovoltaic modules constitutes the fundamental premise upon which passive cooling strategies are based. In comparison to active cooling strategies, the incorporation of phase-change materials (PCMs) into the rear of a photovoltaic (PV) module represents a superior passive cooling solution, as it leads to a reduction in operational and maintenance costs [16]. In a theoretical analysis conducted by Ma et al. [17], it was postulated that the integration of solar thermal modules with PV-PCM devices could potentially lead to a significant enhancement in the overall efficiency of the PV system. Yang et al. [18] undertook a comparative analysis of the thermal and electrical performance of two PVT and PVT-PCM designs. The objective of the laboratory solar simulator experiment was to eliminate the uncertainties associated with outdoor testing, thereby providing a more controlled setting for the experiment. The results demonstrated that the incorporation of capric acid, with a melting point of 30.1 ℃, at the rear of the device panel resulted in a reduction of the back plate temperature by 15.8 ℃. Gan and Xiang [19] put forth a novel configuration for the integration of BIPVT and PCM with building ventilation. It is hypothesized that the device is capable of providing both electricity and natural ventilation. The researchers selected the commercially available salt hydrate PLUSICE S25 (melting temperature of 25°C), composed primarily of calcium chloride dihydrate ($CaCl_2 \cdot 6H_2O$), as it has a high thermal conductivity. The incorporation of a 30 mm layer of PCM was observed to result in an increase in energy production by 10%. In their investigation of the PV-PCM Trombe wall module, Luo et al.[20] examined both a version with and a version without coating of the outer surface of the eutectic PCM layer. The incorporation of PCM had a beneficial impact on the enhancement of photovoltaic performance. It was demonstrated that the incorporation of PCM had a beneficial impact on the enhancement of photovoltaic performance. Concerning BIPV-PCM facades, Cur Pek and Cekon [21] assessed the thermal performance of a BIPV façade module equipped with an RT27 PCM layer and a ventilation system. The authors' analysis focused on the correlation between PCM efficiency and specific climatic variables, with a particular emphasis on ambient air temperature and solar irradiance intensity. The PCM exhibited its optimal performance at midday when solar irradiance values were at their highest. In their studies on the electrical efficiency of various PVT-MCP collectors utilizing five distinct PCMs, Abdelrazik et al. [22] demonstrated that $CaCl_26H_2O$ facilitates a gradual increase in the temperature of the photovoltaic panels, thereby ensuring enhanced electrical efficiency. However, due to its low thermal stability and high-volume expansion, RT35 paraffin wax is the optimal selection. The results of the numerical simulations demonstrate that the PVT-PCM hybrid system outperforms a photovoltaic system operating in isolation. The integration of graphene nano-platelets into the paraffin wax facilitates enhanced cooling of the PV panels and elevates their electrical efficiency.

In light of the aforementioned deliberations, it can be posited that the incorporation of phase change materials (PCMs) within building-integrated photovoltaic (BIPV) systems represents a promising avenue for further exploration. Nevertheless, the diminished thickness of PCM layers in PVT systems constrains their thermal storage capacity [23]. The majority of current numerical simulations focus on partial or simplified structures, which do not fully reflect the energy-saving potential of PCMs when applied to real buildings. Furthermore, a significant number of these studies have been conducted over relatively short periods and under conditions that are representative of the summer season. However, this approach has not fully addressed the

Edelweiss Applied Science and Technology
ISSN: 2576-8484
Vol. 8, No. 6: 2789-2808, 2024
DOI: 10.55214/25768484.v8i6.2558

challenges associated with the low thermal conductivity of PCMs and their tendency to solidify overnight, which can impact their availability and heat dissipation performance the following day [24, 25]. To illustrate, the storage capacity of the PCM could be exceeded by excess heat, which may subsequently affect the interior of the building; conversely, the internal heat generated within the building may also limit the storage capacity of the material. The performance of photovoltaic systems incorporating phase change materials (PCMs, henceforth referred to as PV-PCMs) may be optimized by incorporating additional layers of thermal insulation, thereby regulating the temperature of the PCM and preserving its heat storage capacity [26]. Lin et al. [27] demonstrate that enhancing the insulation of the building's original structure can also enhance the performance of structures incorporating PCMs. Furthermore, the utilization of argon gas serves as an efficacious thermal insulator [28]. To date, no specific study has been conducted on the energy efficiency of a PV-PCM hybrid system in conjunction with a confined argon layer. The impact of this combination on the energy efficiency of BIPVs and indoor thermal comfort remains to be investigated. However, this approach could prove to be a crucial factor in optimizing the performance of BIPV systems.

The present study aims to evaluate the potential gains in energy that may be achieved through the integration of a layer of argon confined to a phase-change material (PCM) positioned at the rear of a photovoltaic panel affixed to a façade. The model will be analyzed using the PV-PCM-argon gap configuration (PVT/ArPCM) and will be compared with a conventional PV-PCM collector (PVT/PCM) to quantify the improvement in terms of photovoltaic cell energy efficiency and indoor thermal comfort.

2. Methodology

2.1. Physical Model

The physical model, illustrated in Figure 1, represents a rectangular cavity with a geometric ratio of A = H/L = 2. It incorporates a phase change material (PCM) and a confined layer of argon, arranged beneath a photovoltaic (PV) panel affixed to the façade of a building. The assembly, designated PVT/ArPCM, serves to regulate the temperature of the photovoltaic cells and provide insulation for the wall, thereby enhancing the thermal environment within the building. A constant heat flow (∅) is applied to the photovoltaic panel, while the right vertical wall is maintained at the ambient temperature (T_{amb}) with its horizontal edges considered adiabatic. The wall of the building was maintained at the melting temperature (T_M) of the PCM to investigate the influence of this parameter on the behaviour of the PCM in the PVT/ArPCM and PVT/PCM configurations. In this study, the electrical efficiency reference is set at 15%, which is the proportion of solar energy that is assumed to be converted into electricity by the photovoltaic panel. The remainder of the energy from the sun is dissipated as heat, transferring to the phase-change material (PCM), which is housed in an aluminum casing below the panel. It is assumed that the model is two-dimensional and that the two fluids (argon and air) are Newtonian and incompressible.

Edelweiss Applied Science and Technology
ISSN: 2576-8484
Vol. 8, No. 6: 2789-2808, 2024
DOI: 10.55214/25768484.v8i6.2558

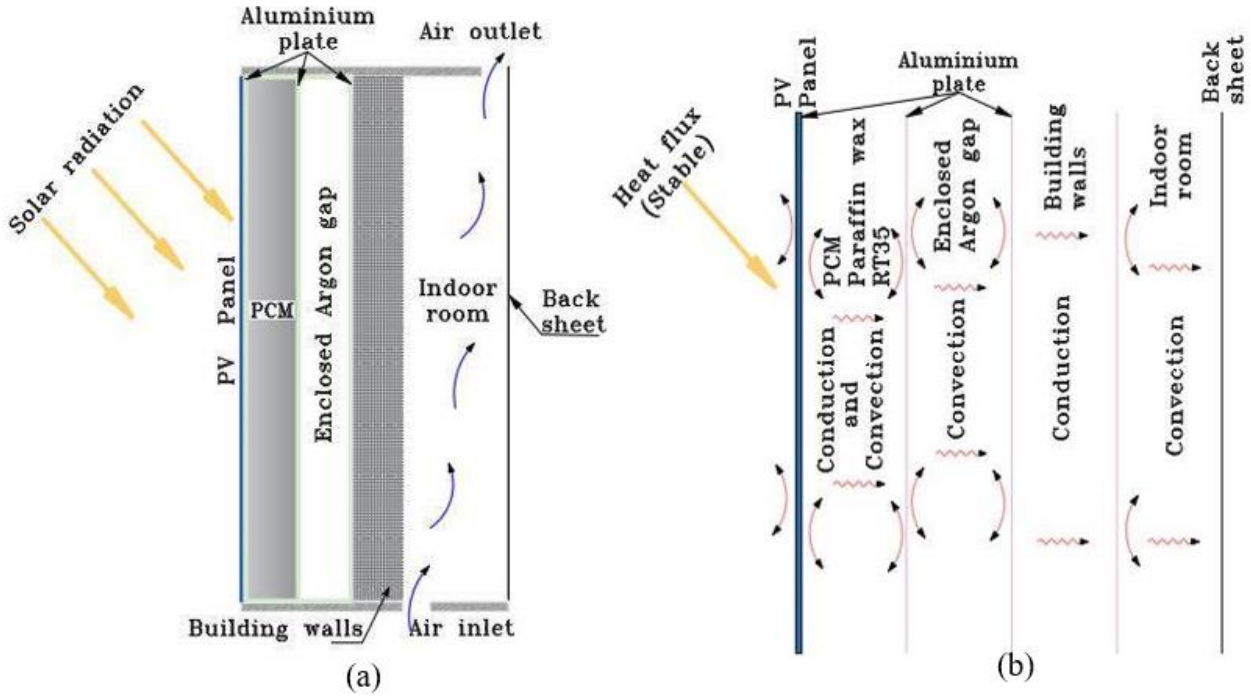

Figure 1.
(a) Schematic diagram of the system, (b) Heat transfer flow chart through the system.

The argon confined within the insulation cavity is characterized by thermal conductivity (λ_{Ar}) and a convection coefficient (h_{Ar}). Conversely, the air circulating within the building is characterized by thermal conductivity, λ_{Air}, and a convection coefficient, h_{Air}. Table 1 presents the thermal and rheological properties of the materials employed. RT35 paraffin wax was selected for its commercial availability, widespread use, and non-combustible, non-corrosive properties, thereby ensuring safe use in aluminum housing [29]. It was postulated that the fluid flow would be laminar and stable. The thermophysical properties of the fluids, as illustrated in Table 1, were assumed to be constant, except for density, which was modeled using the Boussinesq approximation for the gravitational term.

Table 1.
Thermal and rheological properties of the materials used in the study.

Thermo-physical properties	PCM Paraffin wax RT35	Aluminium	Argon	Air
Melting point (°C)	29-36	-	-	-
Heat of fusion (kJ.kg^{-1})	130 [29]	-	-	-
Thermal conductivity (W.m^{-1}. °C^{-1})	0.2 [29]	202.4 [29]	0.017[30]	0.025 [30]
Density (kg.m^{-3})	800 [29]	2791 [29]	1.70 [30]	1.23 [30]
Specific heat capacity (J.kg^{-1}K^{-1})	2000 [29]	871 [29]	519 [30]	1008 [30]
Emissivity	-	0.095 [29]	-	-

This study excludes the consideration of radiation due to the significant influence it exerts upon temperature variations below 100°C [31]. Moreover, the mean temperatures of photovoltaic cells equipped with heat exchangers, even when exposed to maximum irradiation levels of 1,000 W/m², are

Edelweiss Applied Science and Technology
ISSN: 2576-8484
Vol. 8, No. 6: 2789-2808, 2024
DOI: 10.55214/25768484.v8i6.2558

typically observed to be below 40°C [32]. This observation serves to reinforce the argument for the exclusion of radiation from the analytical framework.

2.2. Mathematical Models

This study is a computational fluid dynamics (CFD) modelling study that incorporates four main components. The first of these is the convection model for the fluids, which includes the confined argon and air flowing in the building. The second is the heat transfer model in the building wall. The third is the phase change model for the phase change material (PCM), and the fourth is the energy production model.

2.3. Fluid Model

The dimensionless equations for two-dimensional incompressible laminar flow, namely those governing continuity, momentum, and energy, are as follows:

$$\frac{\partial U}{\partial X}+\frac{\partial V}{\partial Y}=0 \tag{1}$$

$$\frac{\partial \Omega}{\partial \tau}+U\frac{\partial \Omega}{\partial X}+V\frac{\partial \Omega}{\partial Y}=\frac{R_a}{P_r R_e^2}\frac{\partial \theta}{\partial X}+\frac{1}{Re}\left(\frac{\partial^2 \Omega}{\partial X^2}+\frac{\partial^2 \Omega}{\partial Y^2}\right) \tag{2}$$

$$\frac{\partial \theta}{\partial \tau}+U\frac{\partial \theta}{\partial X}+V\frac{\partial \theta}{\partial Y}=\frac{1}{R_e P_r}\left(\frac{\partial^2 \theta}{\partial X^2}+\frac{\partial^2 \theta}{\partial Y^2}\right) \tag{3}$$

$$\Omega=-\left(\frac{\partial^2 \Psi}{\partial X^2}+\frac{\partial^2 \Psi}{\partial Y^2}\right) \tag{4}$$

The stream function and vorticity are related to the velocity components by the following expressions: $U=\frac{\partial \Psi}{\partial Y}\ ;V=-\frac{\partial \Psi}{\partial X}\ ;\ \Omega=\frac{\partial V}{\partial X}-\frac{\partial U}{\partial Y}$ (5)

2.3.1. Heat Transfer Model

In addition to generating electrical power, a substantial portion of the solar radiation absorbed by the photovoltaic (PV) module is transferred to a phase change material (PCM), where it is transformed into heat. It is assumed that heat loss from the PV-PCM system to the outside environment is negligible due to the presence of adiabatic horizontal walls. The heat conduction within the solid component of the system, comprising the solid phase change material and the external wall of the building, is given by the following expression.

$$\frac{\partial \theta}{\partial \tau}=\frac{a_r}{R_e P_r}\left(\frac{\partial^2 \theta}{\partial X^2}+\frac{\partial^2 \theta}{\partial Y^2}\right) \tag{6}$$

a_r is the relative diffusivity of each solid.

2.3.2. Phase Change Model

The dimensionless form of the solid/liquid interface equation is defined in terms of the Stefan number:

$$\left(\frac{\partial \theta_l}{\partial n}\right)-\frac{\lambda_s}{\lambda_l}\left(\frac{\partial \theta_s}{\partial n}\right)=\frac{St}{Re}\left(\frac{\partial \zeta}{\partial \tau}\right) \tag{7}$$

With ζ the liquid fraction is defined as: $\zeta=\begin{cases}0 & \theta<\theta_M\\ 0-1 & \theta=\theta_M\\ 1 & \theta>\theta_M\end{cases}$ (8)

Edelweiss Applied Science and Technology
ISSN: 2576-8484
Vol. 8, No. 6: 2789-2808, 2024
DOI: 10.55214/25768484.v8i6.2558

2.3.3. Initial and Boundary Conditions

Initial conditions: at $\tau = 0\ ;\ \theta = \Omega = \Psi = U = V = 0;\ \theta_{wall} = \theta_M$ (9)

at $\tau > 0$, The boundary conditions associated with the problem are found below:

$$X = 0;\ 0 < Y < A; U = V = \Psi = 0\ ;\ \Omega = -\left.\frac{\partial^2\Psi}{\partial X^2}\right|_{X=0}; -\left.\frac{\partial\theta}{\partial X}\right|_{X=0} = \tau_{pv}\alpha_{pv}\tau_{Al}\alpha_{Al} - \eta_e \quad (10)$$

$$X = B_1;\ 0 < Y < A; U = V = \Psi = 0\ ; \Omega = -\left.\frac{\partial^2\Psi}{\partial X^2}\right|_{X=B_1}; -\left.\frac{\partial\theta}{\partial X}\right|_{X=B_1} = \tau_{pv}\alpha_{pv}\tau_{Al}^2\alpha_{Al}^2 - ABi_1\theta_{PCM} \quad (11)$$

$$X = B_2;\ 0 < Y < A; U = V = \Psi = 0\ ;\ \Omega = -\left.\frac{\partial^2\Psi}{\partial X^2}\right|_{X=B_2};\quad -\left.\frac{\partial\theta}{\partial X}\right|_{X=B_2} = \tau_{pv}\alpha_{pv}\tau_{Al}^3\alpha_{Al}^3\alpha_{wall} + ABi_2\theta_{wall} \quad (12)$$

$$X = B_3;\ 0 < Y < A; U = V = \Psi = 0\ ;\ \Omega = -\left.\frac{\partial^2\Psi}{\partial X^2}\right|_{X=B_2};\quad -\left.\frac{\partial\theta}{\partial X}\right|_{X=B_2} = \tau_{pv}\alpha_{pv}\tau_{Al}^3\alpha_{Al}^3\alpha_{wall}\tau_{wall} - ABi_3\theta_{wall} \quad (13)$$

$$X = 1;\ 0 < Y < A; U = V = \theta = 0\ ; \Psi = -B_4 + 1,\ \Omega = -\left.\frac{\partial^2\Psi}{\partial X^2}\right|_{X=1} \quad (14)$$

$$Y = 0;\ 0 < X < B_3\ ; U = V = \Psi = 0\ ; \Omega = -\left.\frac{\partial^2\Psi}{\partial Y^2}\right|_{Y=0};\ \left.\frac{\partial\theta}{\partial Y}\right|_{Y=0} = 0 \quad (15)$$

$$Y = 0;\ B_3 < X < B_4; U = \theta = 0; V = 1; \Psi = -X + 1; \Omega = -\left.\frac{\partial^2\Psi}{\partial Y^2}\right|_{Y=0} \quad (16)$$

$$Y = 0;\ B_4 < X < 1; U = V = 0\ ; \Psi = -B_4 + 1;\ \Omega = -\left.\frac{\partial^2\Psi}{\partial Y^2}\right|_{Y=0};\ \left.\frac{\partial\theta}{\partial Y}\right|_{Y=0} = 0 \quad (17)$$

$$Y = A;\ 0 < X < B_5;\ U = V = \Psi = 0\ ;\ \Omega = -\left.\frac{\partial^2\Psi}{\partial Y^2}\right|_{Y=A};\ \left.\frac{\partial\theta}{\partial Y}\right|_{Y=A} = 0 \quad (18)$$

$$Y = A;\ B_4 < X < 1\ ;\ U = 0\ ; \left.\frac{\partial V}{\partial Y}\right|_{Y=A} = \left.\frac{\partial\Psi}{\partial Y}\right|_{Y=A} = \left.\frac{\partial\Omega}{\partial Y}\right|_{Y=A} = \left.\frac{\partial\theta}{\partial Y}\right|_{Y=A} = 0 \quad (19)$$

2.3.4. Power generation model

As a consequence of the elevated temperature of the cells, the electric power produced by the PVT system is expressed by the following equation:

$$P_{el} = P_{ref}[1 - \beta_{PV}(T_{PV} - T_{amb})]\ [33] \quad (20)$$

The relationship between increasing temperature and decreasing photovoltaic efficiency is expressed by the following equation:

$$\eta_{el} = \eta_{ref}[1 - \beta_{PV}(T_{PV} - T_{amb})]\ [34] \quad (21)$$

The average absolute PV panel temperature is defined by:

$$T_{PV} = \frac{1}{H}\int_0^H T_{PV}(y)dy \quad (22)$$

The temperature of solar cells is dependent upon ambient conditions, and can be calculated utilizing the following formula:

$$T_{PV} = T_{amb} + \left(\frac{NOCT - 20^\circ}{0.8}\right)G\ [33].\quad \text{G is the insolation (kW/m}^2\text{).} \quad (23)$$

The mean Nusselt number observed along the length of the PV cell plate is:

$$Nu_{PV} = \frac{1}{H}\int_0^H \frac{1}{\theta_{PV}(y)}dy \quad (24)$$

Table 2.
Numerical model input parameters.

Parameters	Values
Absorptivity of PV cells surface, $\boldsymbol{\alpha_{pv}}$	0.95 (-)
Transmittance of PV cells surface, $\boldsymbol{\tau_{pv}}$	0.09 (-)
Maximum rated power, $\boldsymbol{P_{rated}}$	150 W

Edelweiss Applied Science and Technology
ISSN: 2576-8484
Vol. 8, No. 6: 2789-2808, 2024
DOI: 10.55214/25768484.v8i6.2558

Temperature coefficient of PV cell, β_{PV}	0.48%/◦ C [33]
Reference value for electrical efficiency, η_{ref}	0.015(-)
Nominal Operating Cell Temperature, NOTC	48°C [33]
Ambient Temperature, T_{amb}	25°C
Incoming Solar Flux, G	200-850 W/m²
Coefficient of heat transfer from wall to air	$h_{air}=5.62+3.9V_{wind}$ [35]
Coefficient of heat transfer from PCM to argon gap	$h_{Ar1}= \Phi / \lvert T_{Ar}-T_{PCM} \rvert$ [36]
Coefficient of heat transfer from Wall to argon gap	$h_{Ar1}= \Phi / \lvert T_{Wall}- T_{Ar} \rvert$ [36]

3. Numerical Procedure

To obtain a discrete solution to the nonlinear partial differential equations (1-3), an implicit finite difference method was employed. The first and second derivatives of the diffusive terms were approximated using centered finite differences, while a second-order scheme was employed to approximate the convective terms to prevent the potential instabilities often encountered in mixed convection flow problems. The differential equations were transformed into a linear algebraic system, which was subsequently solved using the Thomas algorithm. At each time step, the Poisson equation (4) was solved using the successive point sub-relaxation (PSUR) method with an optimal sub-relaxation coefficient of 0.8, as this proved optimal for the (201×41) grid used in the study. The principal benefit of this methodology lies in its utilization of the Gauss-Seidel approach to facilitate the attainment of an intermediate iterate, which will henceforth be designated as ϕ^{k+1}, Subsequently, the method is "relaxed" to accelerate convergence. Moreover, the Gauss-Seidel method is a relatively simple one to implement in a programming environment. Convergence of the iteration for the stream function solution was achieved at each time step, and a criterion was employed to ascertain the existence of a steady-state solution. Convergence of solutions is deemed to have been achieved when the relative error for each variable between consecutive iterations is less than the convergence criterion, such that $\varepsilon = \sum \lvert (\phi_i^k{}_j^{+1} - \phi_i^k{}_j) / \phi_i^k{}_j^{+1} \rvert < 10^{-5}$ where ϕ stands for ψ, θ, ω, k refers to time and i and j refer to space coordinates. In the computations, a time step of size 10^{-5} is utilized.

To mitigate the impact of the mesh on the accuracy of the simulation, a mesh independency solution was employed, whereby the influence of the grid mesh on the highest Rayleigh and Reynolds numbers (Ra=5106, Re=1) used in the present study was assessed. As illustrated in Table 1, the non-uniform 101x51 and 201x101 meshes show minor inconsistencies in the characteristic quantities Ψ, θ, and Nu compared to the uniform 101x101 and 201x201 meshes.

Adopting an irregular grid optimizes resolution, providing an improved geometric representation of the model and reducing the incidence of numerical errors while enhancing computational efficiency. Nevertheless, the 201x101 mesh was chosen because it is more effective in transmitting heat than the 101x51 mesh, as demonstrated by a 1.68% increase in the Nusselt number.

Table 3.
Grid Independency.

Stage	Ψmax	Change (%)	θmax	Change (%)	Numax	Change (%)
101X51	-0.220	˜	0.026	˜	20.52	˜
201X101	-0.209	5	0.025	3.84	20.87	1.68
101X101	-0.060	˜	0.00009	˜	10.70	˜
201X201	-0.010	83.33	0.00004	55.55	15.72	2

Edelweiss Applied Science and Technology
ISSN: 2576-8484
Vol. 8, No. 6: 2789-2808, 2024
DOI: 10.55214/25768484.v8i6.2558

The vorticity computational formula proposed by Woods [37] was employed to approximate wall vorticity: $\Omega(w) = \frac{1}{2}\Omega_{w+1} - \frac{3}{\Delta\eta^2}(\psi_{w+1} - \psi_w)$, The stream function values ψw and ψw+1 are taken at the points adjacent to the boundary wall, while η represents the normal abscise on the boundary wall.

4. Results and Discussion

4.1. Validation

As the thermal properties of the phase-change material (PCM) layer and the argon layer are fundamental to the performance of the photovoltaic (PV) panel and the thermal comfort of the indoor environment, it is imperative to validate the numerical model. In the lack of published data for a comparable system, two aspects have been validated independently. The first concerns the validation of the natural convection phase change model employed to simulate heat transfer within the PCM and the fluid cavity. The second assesses the accuracy of the equations used to describe the heat transfer between the PCM, the PV panel, and the backplate. A comparison was conducted between the results obtained and the findings reported in the studies by Noureddine et al.[38], Ma et al.[29], and Abdelrazik et al.[22].

4.1.1. Validation of the Natural Convection Phase-Change Model

In their study, Noureddine et al. investigated the phenomenon of heat transfer by natural convection during the melting of an organic phase-change material.

Edelweiss Applied Science and Technology
ISSN: 2576-8484
Vol. 8, No. 6: 2789-2808, 2024
DOI: 10.55214/25768484.v8i6.2558

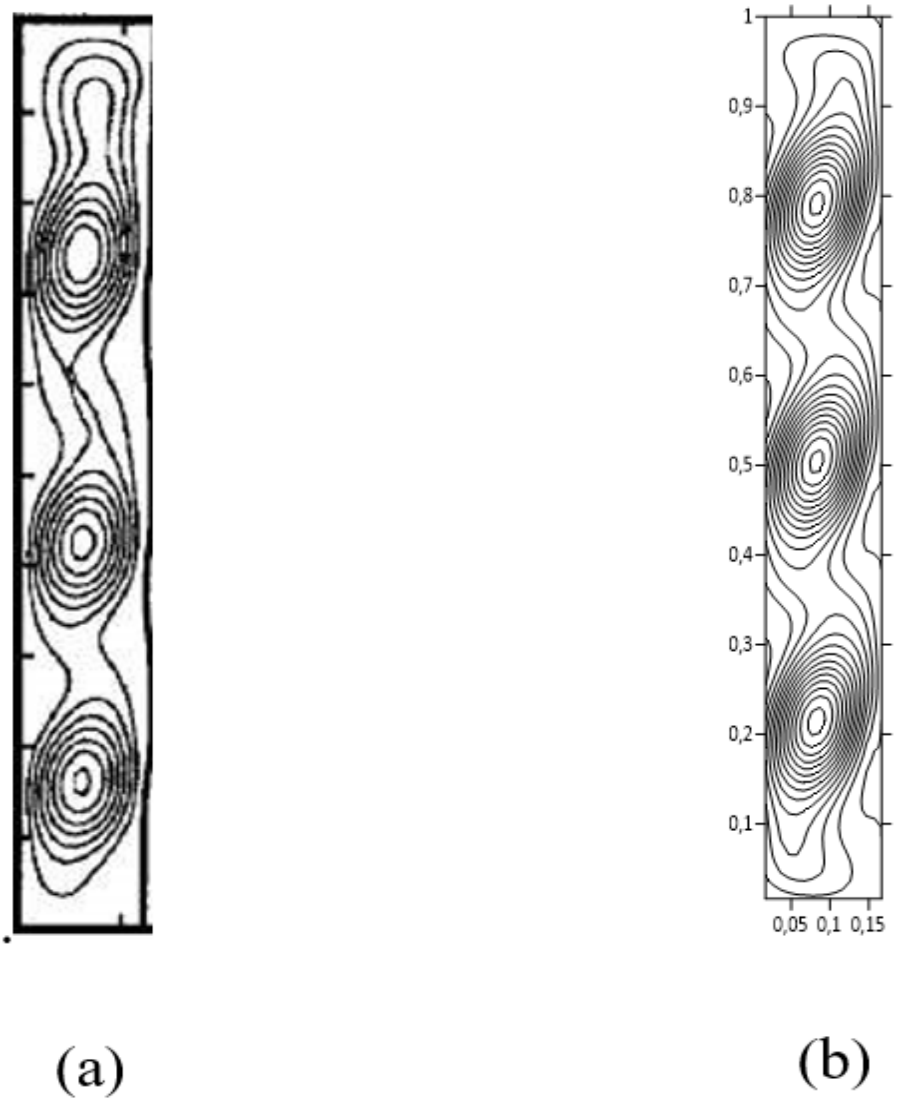

Figure 2.
Comparison of the streamlines of (a) the present work with those of (b) Noureddine et al.[38].

Edelweiss Applied Science and Technology
ISSN: 2576-8484
Vol. 8, No. 6: 2789-2808, 2024
DOI: 10.55214/25768484.v8i6.2558

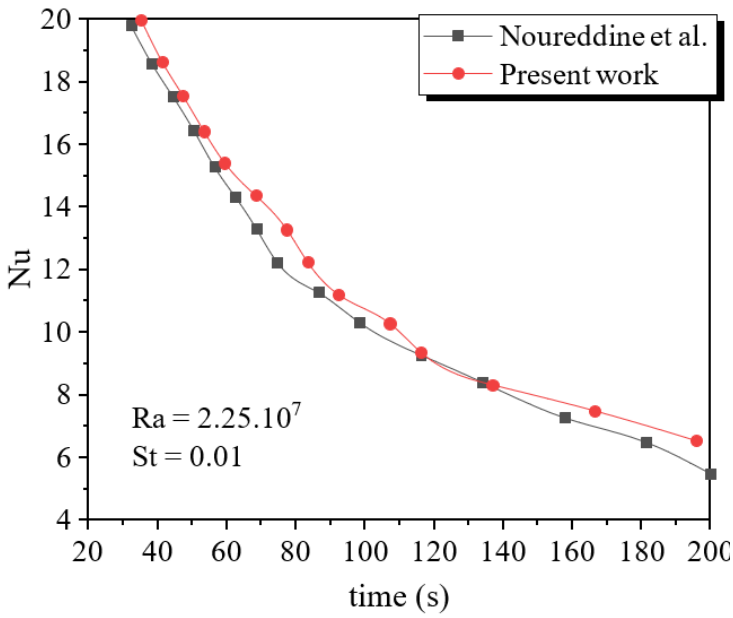

Figure 3.
Comparison of average Nusselt number.

A comparison of streamline patterns was conducted for a set of parameters comprising a Raleigh number, Ra = 2.25×10^5, Stefan number St = 0.01, and Re =1 (pure natural convection). These were observed after a 200-second simulation period and demonstrated a high degree of agreement (Figure 2). The evolution of the average Nusselt number along the PV module as a function of time for the model developed in this study (Figure 3) exhibited a high degree of concordance, with the percentage error falling below 3%.

4.1.2. Validation of the PV/PCM Model

Edelweiss Applied Science and Technology
ISSN: 2576-8484
Vol. 8, No. 6: 2789-2808, 2024
DOI: 10.55214/25768484.v8i6.2558

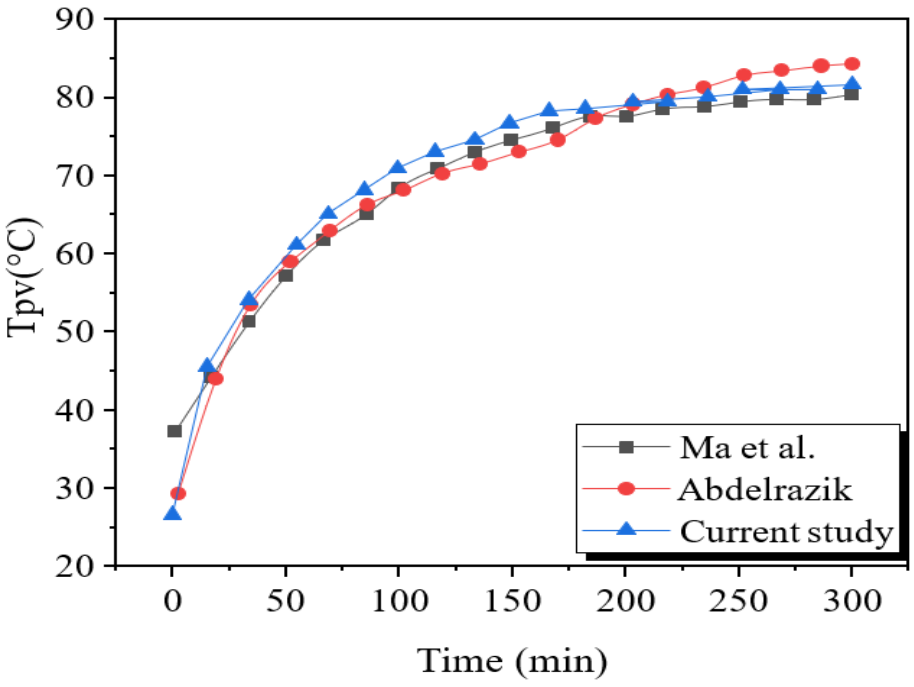

Figure 4.
Comparison of PV temperatures with those of Ma et al.[29] and Abdelrazik et al.[22].

The PV/PCM model developed in this study was validated using the model of Ma et al. [29] which was also used by Abdelrazik et al. [22]. They used the PCM Paraffin wax RT35, the properties of which are presented in Table 1, and evaluated the performance of the system under atmospheric conditions of 35°C, solar radiation of 1000 W/m², and in the absence of wind. The temporal evolution of the PV module temperature, simulated using the model developed, shows remarkable agreement with an error deviation of less than 3%, as shown in Figure 4.

4.1.3. Effect of the Argon Layer on the Thermal Management of the PV /PCM System

Figure 5 depicts the influence of the argon layer on the thermal flow and distribution following a three-hour exposure period. In the confined channel, natural convection based on the principle of buoyancy provides a stable thermal flow which optimizes the transfer of heat from the photovoltaic (PV) cells to the phase-change material (PCM), as demonstrated by Akshayveer et al. [39]. In the PVT/PCM system, the dissipation of heat between the building wall and the PCM is more pronounced, accelerating the PCM melting process and resulting in the formation of large rotating cells (Ψmax: 30 > 20), a phenomenon also observed by Moench et al. [40]. In contrast, in the PVT/ArPCM system, the melting of the PCM is slower, which allows for more effective thermal management of the phase-change material, which is capable of storing more heat (θmax: 0.12 > 0.1).

Edelweiss Applied Science and Technology
ISSN: 2576-8484
Vol. 8, No. 6: 2789-2808, 2024
DOI: 10.55214/25768484.v8i6.2558

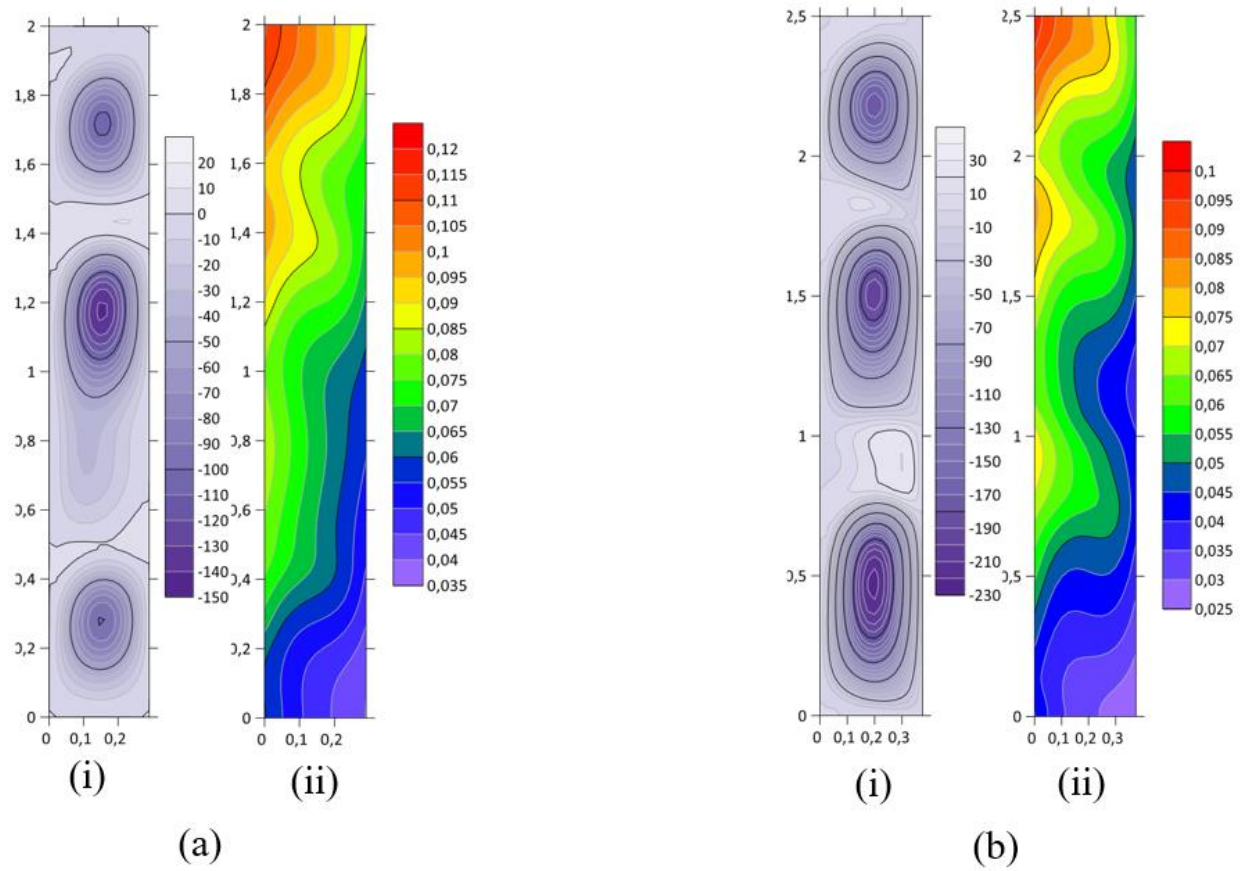

Figure 5.
Streamlines (i) and isotherms (ii) after 3H of operation (a) PVT/ArPCM and (b) PVT/PCM.

As illustrated in Figure 6, the implementation of an argon thermal shield has been found to exert a considerable influence on the trajectory of the mean temperature of a photovoltaic panel over an extended period. The observed temperature variations can be attributed to the distinctive thermophysical properties of argon (as detailed in Table 2), as elucidated by Tobechi et al. [41]. The low thermal conductivity of argon serves to reduce the transfer of heat from the building envelope to the phase-change material (PCM), thereby facilitating the cooling of the photovoltaic panel due to its thermal resistance to heat flow from the envelope. Conversely, the high thermal conductivity of the building envelope (concrete) results in an increase in the internal temperature of the phase-change material (PCM), which directly influences the temperature of the photovoltaic cells. An investigation into the thermal evolution of the photovoltaic (PV) module has revealed a reduction of 1.35 degrees Celsius in temperature for the PVT/ArPCM system when compared with the conventional PVT/PCM system.

Edelweiss Applied Science and Technology
ISSN: 2576-8484
Vol. 8, No. 6: 2789-2808, 2024
DOI: 10.55214/25768484.v8i6.2558

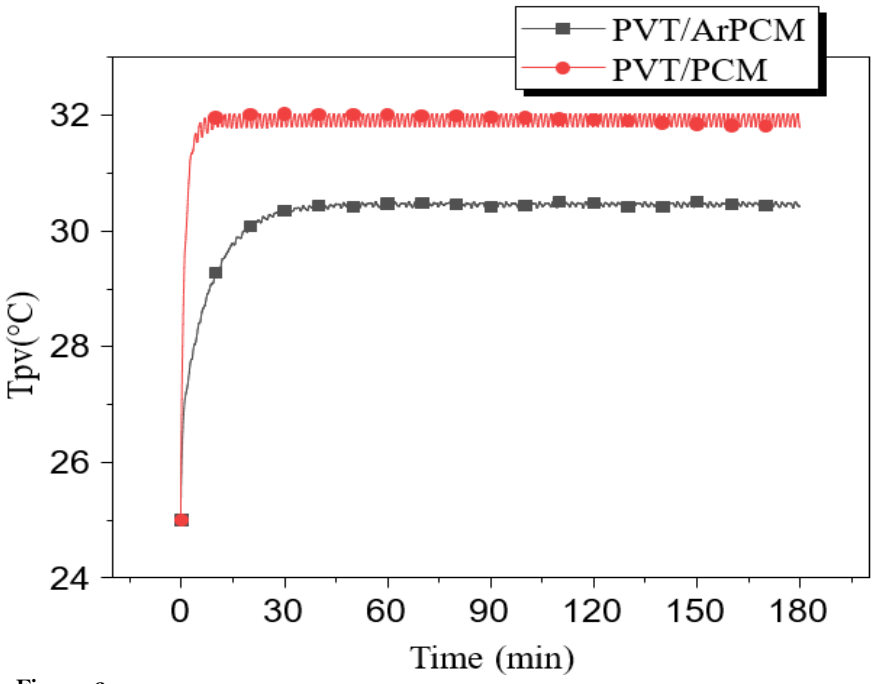

Figure 6.
Temperature distribution of PV panel.

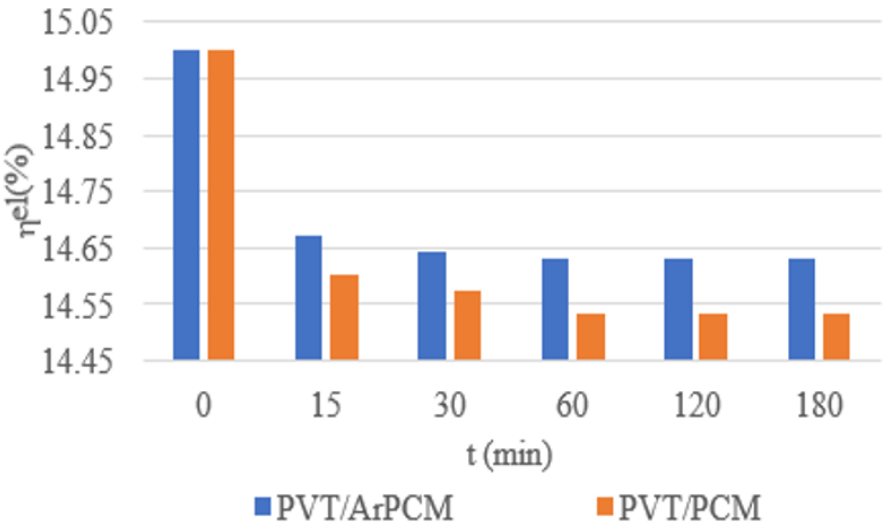

Figure 7.
Electrical efficiency for three hours of operation.

As can be observed in Figure 7, the electrical efficiency of the system is influenced by changes in the temperature of the solar panel. The integration of an argon-based heat shield into the PVT/ArPCM system results in the highest levels of electrical efficiency. However, the use of RT 35 paraffin wax as PCM provides effective thermal management. This observation is supported by the findings of Abdelrazik et al. [22], which confirm the thermal efficiency of the PCM in comparable systems. A 0.10% improvement in electrical efficiency was observed for the PVT/ArPCM system in comparison with the conventional PVT/PCM system.

Edelweiss Applied Science and Technology
ISSN: 2576-8484
Vol. 8, No. 6: 2789-2808, 2024
DOI: 10.55214/25768484.v8i6.2558

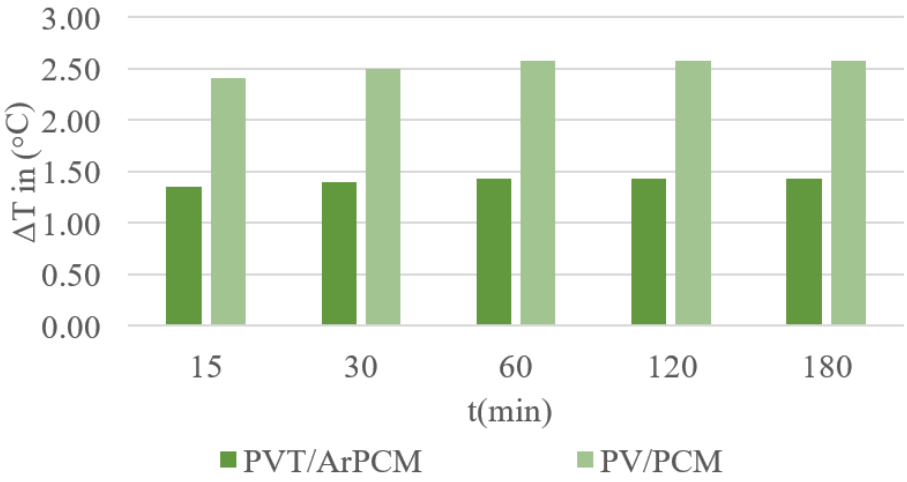

Figure 8.
Variation in average indoor temperature for 3 hours of operation.

Figure 8 demonstrates that after three hours, the maximum temperature fluctuation within the building was 1.43°C for system PVT/ArPCM, compared to 2.57°C for system PVT/PCM. This reduction in thermal amplitude signifies a 44% enhancement in thermal comfort performance. This improvement can be attributed to the excellent insulating properties of argon, as evidenced by the findings of Lolli et al. [28].

4.2. *Energy Analysis of the PVT/PCM System with Argon Layer Under Different Irradiances.*

A comparative assessment of the performance of the PVT/ArPCM system and the conventional PVT/PCM system was conducted through the examination of the two configurations under different irradiances.

Table 4.
Electrical performance of PV cells and building thermal comfort.

Irradiance W/m2	**300**		**500**		**680**		**850**	
System	**PVT/ ArPCM**	**PVT/ PCM**	**PVT/ ArPCM**	**PVT/ PCM**	**PVT/ ArPCM**	**PVT/ PCM**	**PVT/ ArPCM**	**PVT/ PCM**
$T_{PV_{MOY}}max$ (°C)	36.08	37.09	42.10	42.11	48.28	48.31	54.90	54.91
Change (%)	2.72	~	0.023	~	0.06	~	0.018	~
$P_{el}min$ (W)	142.03	141.29	137.70	137.68	133.24	133.22	128.47	128.45
Change (%)	0.52	~	0.014	~	0.015	~	0.015	~
$\eta_{elmoy}min$ (%)	14.25	14.18	13.85	13.83	13.43	13.41	12.98	12.97
Change (%)	0.07	~	0.02	~	0.02	~	0.01	~
$\Delta T_{ind}max$ (°C)	1.44	4.14	1.45	4.16	1.45	4.19	1.47	4.21
Change (%)	65.69	~	65.14	~	65.39	~	65.08	~

The analysis was conducted to determine the output of the photovoltaic cells in terms of electricity generated, the efficiency with which they performed, and the level of thermal comfort experienced by occupants of the building. Such assessments permitted the quantification of the thermal and energy impact of the system as a function of irradiance variations, thereby facilitating a more nuanced comprehension of its behaviour under diverse solar exposure conditions. The two configurations were then subjected to an in-depth examination of their thermoelectric performance, the findings of which are

Edelweiss Applied Science and Technology
ISSN: 2576-8484
Vol. 8, No. 6: 2789-2808, 2024
DOI: 10.55214/25768484.v8i6.2558

presented in Table 4. In general, there is a discernible decline in electrical performance as irradiance levels increase. A minimum improvement of 0.018% in solar cell cooling, 0.014% in electrical power supplied, and 0.01% in electrical efficiency is observed for the PVT/ArPCM collector in comparison to the PVT/PCM collector. Furthermore, Table 4 illustrates the effects of the two configurations on the internal temperature of the building under identical solar irradiation conditions. The PVT/ArPCM configuration exhibits a minimum improvement in thermal comfort of 65%.

4.3. Analysis of Thermal Management of RT-35 PCMs in Each of the 2 Configurations

The objective of the study, as depicted in Figure 9, is to analyze the thermal storage management of the phase-change materials (PCMs) in the two configurations.

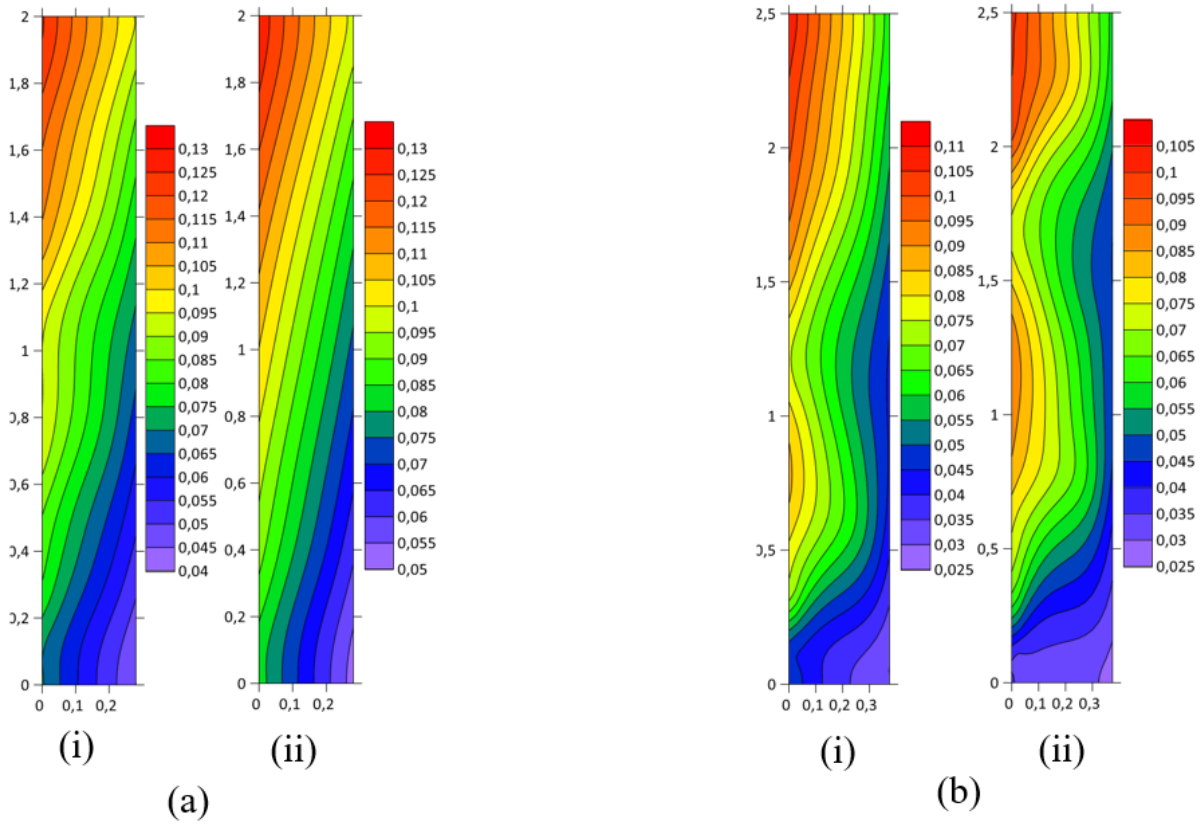

Figure 9.
Distribution of isotherms at (i) the end of the imposed solar flux and (ii) two hours later; (a) PVT/ArPCM and (b) PVT/PCM.

Two hours after the cessation of the solar flux, the maximum dimensionless temperature of the PCM remained stable in the PVT/ArPCM configuration, while the minimum dimensionless temperature exhibited a change, indicating enhanced thermal management. In contrast, in the PVT/PCM configuration, the maximum dimensionless temperature of the PCM exhibited a decline of 0.05, indicating a reduction in performance following the cessation of the imposed solar flux.

5. Conclusion

To ascertain the efficacy of photovoltaic (PV) cells when integrated into a building's façade, a numerical model comprising an argon-based thermal screen was designed and analyzed This model enabled the electrical production of the PV cells, their efficiency, and variations in the temperature

Edelweiss Applied Science and Technology
ISSN: 2576-8484
Vol. 8, No. 6: 2789-2808, 2024
DOI: 10.55214/25768484.v8i6.2558

within the building to be evaluated. This was done in conjunction with a conventional PV/PCM (Phase-Change Material) system installed on the façade, under different irradiation conditions. Additionally, the thermal storage performance of the phase-change materials (PCMs) in each configuration was investigated. The principal findings of this analysis are as follows:

- The PVT system demonstrated a slight enhancement in electrical efficiency, with a 0.01% increase. Additionally, the incorporation of an argon-filled thermal screen resulted in a notable 65% improvement in indoor thermal comfort.
- A marginal reduction in PV cell temperature of 0.01°C was observed with the argon layer.
- The electrical power output exhibited a slight improvement of 0.014% in the presence of argon.
- The thermal management of the PVT/ArPCM collector was observed to be more effective than that of the PVT/PCM collector, as evidenced by the superior thermal performance of the PCM utilized in the former.

A comprehensive numerical study is currently being undertaken to exploit the heat stored in the PCM. This study will evaluate the thermal and electrical performance of the collector over a full year under tropical climate conditions.

Nomenclature

letters

a_r	:	Relative thermal diffusivity ($a_r = \frac{\lambda_r}{\rho_r Cp_r}$)
B_1	:	Aspect ratio between the width of PCM layer and width of the collector ($B_1 = \frac{e_{PCM}}{L}$)
B_2	:	Aspect ratio of argon layer width to collector width ($B_1 = \frac{e_{argon\ layer}}{L}$)
B_{i1}	:	Biot number of Argon ($B_{i1} = \frac{h_{Ar}L}{\lambda_{Al}}$)
B_{i2}	:	Biot number of Air ($B_{i2} = \frac{h_{Air}L}{\lambda_{Wall}}$)
Cp	:	Specific heat (J. Kg^{-1}. K^{-1})
g	:	Gravity acceleration (m.s^{-2})
h	:	Convective transfer coefficient (W m^{-2}K^{-1})
H	:	Height of collector (m)
L	:	Length of collector (m)
Pr	:	Prandtl number ($Pr = \frac{\mu c_p}{\lambda}$)
Ra	:	Rayleigh number ($Ra = \frac{\rho^2 g\beta\emptyset L^4}{\lambda\mu^2}$)
Re	:	Reynolds number ($Re = \frac{\rho V_0 L}{\mu}$)
St		Stefan number ($Ste = \frac{Cp(T_M - T)}{L}$)
t	:	Temps (s)
T	:	Temperature (K)
u, v	:	Velocity components in x and y directions (m.s^{-1})
U, V	:	Dimensional components of velocity in X and Y directions ($U = \frac{u}{v_0}$; $V = \frac{v}{v_0}$)
v_0	:	Air inlet velocity in the lower channel of the chimney (m.s^{-1})
X, Y	:	Dimensionless Cartesian coordinates ($X = \frac{x}{L}$; $Y = \frac{y}{L}$)
x, y	:	Cartesian coordinates (m)

Greek letters

α	:	Absorptivity coefficient (-)
β	:	Coefficient of thermal expansion (K^{-1})

Edelweiss Applied Science and Technology
ISSN: 2576-8484
Vol. 8, No. 6: 2789-2808, 2024
DOI: 10.55214/25768484.v8i6.2558

$\mathbf{\Delta T_{ind}}$	:	Variation in average indoor temperature (°C)
$\mathbf{\Omega}$	:	Dimensionless vorticity ($\Omega = \frac{\omega v_0}{L}$)
$\boldsymbol{\omega}$	:	Dimensional vorticity (s^{-1})
$\boldsymbol{\psi}$	:	Dimensional stream function ($m^2.s^{-1}$)
$\mathbf{\Psi}$	:	Dimensionless stream function ($\Psi = \frac{\psi}{Lv_0}$)
$\mathbf{\Theta}$	:	Dimensionless temperature ($\theta = \lambda\left(\frac{T-T_a}{\phi L}\right)$)
$\boldsymbol{\tau}$	:	Dimensionless time ($\tau = \frac{v_0}{L} t$)
$\boldsymbol{\lambda}$	:	Thermal Conductivity Coefficient ($W.m^{-1}. K^{-1}$)
$\boldsymbol{\mu}$	:	Air dynamic viscosity ($Kg.m^{-1}. s^{-1}$)
$\boldsymbol{\rho}$	:	Density ($Kg.m^{-3}$)
$\boldsymbol{\tau}$	:	Transmission coefficient (-)

Indices

Al	:	Aluminium
Ar	:	Argon
M	;	Melt
$\boldsymbol{pv}$	:	Photovoltaic
r	:	Relative

Funding:
This work has been supported by the Regional Center of Excellence for Electricity Management (CERME).

Acknowledgments:
This work was supported by the Regional Centre of Excellence on Electricity Management (CERME) at the University of Lomé. With these words, the authors express their gratitude to the CERME.

Author Contributions:
K.A.T. worked on the research paper, YDL, KK participated in proofreading the paper and YN carried out supervision. All authors have read and accepted the published version of the manuscript.

References

[1] X. Cao, X. Dai, and J. Liu, "Building energy-consumption status worldwide and the state-of-the-art technologies for zero-energy buildings during the past decade," *Energy Build*, vol. 128, pp. 198–213, Sep. 2016, doi: 10.1016/j.enbuild.2016.06.089.

[2] R. Azari, E. Kamel, and A. M. Memari, "Current Developments and Future Directions in Energy-Efficient Buildings from the Perspective of Building Construction Materials and Enclosure Systems," Jul. 01, 2024, *Multidisciplinary Digital Publishing Institute (MDPI)*. doi: 10.3390/buildings14071921.

[3] K. J. Chua, S. K. Chou, W. M. Yang, and J. Yan, "Achieving better energy-efficient air conditioning - A review of technologies and strategies," 2013, *Elsevier Ltd*. doi: 10.1016/j.apenergy.2012.10.037.

[4] A. Kitsopoulou, E. Bellos, and C. Tzivanidis, "An Up-to-Date Review of Passive Building Envelope Technologies for Sustainable Design," Aug. 01, 2024, *Multidisciplinary Digital Publishing Institute (MDPI)*. doi: 10.3390/en17164039.

[5] T. Katsura, S. Memon, A. Radwan, M. Nakamura, and K. Nagano, "Thermal performance analysis of a new structured-core translucent vacuum insulation panel in comparison to vacuum glazing: Experimental and theoretically validated analyses," *Solar Energy*, vol. 199, pp. 326–346, Mar. 2020, doi: 10.1016/j.solener.2020.02.030.

[6] H. M. Maghrabie, K. Elsaid, E. T. Sayed, M. A. Abdelkareem, T. Wilberforce, and A. G. Olabi, "Building-integrated photovoltaic/thermal (BIPVT) systems: Applications and challenges," *Sustainable Energy Technologies and Assessments*, vol. 45, Jun. 2021, doi: 10.1016/j.seta.2021.101151.

[7] A. Hasan, S. J. McCormack, M. J. Huang, and B. Norton, "Energy and cost saving of a photovoltaic-phase change materials (PV-PCM) System through temperature regulation and performance enhancement of photovoltaics," *Energies (Basel)*, vol. 7, no. 3, pp. 1318–1331, 2014, doi: 10.3390/en7031318.

[8] E. H. A. Mohammed, E. Z. Mohamed, K. A.E., K. Abdelkrim, I. Kashif, and R. Shafiqur, "Numerical analysis and design of a novel solar photovoltaic thermal system using finned cooling channel structures embedded with air/TiO2–water nano bi-fluid," *Solar Energy*, vol. 269, Feb. 2024.

[9] Y. Nougbléga, K. Kpode, K. Atchonouglo, M. Banna, and J. C. Dupé, "Effect of enclosed air gap and empty gap for thermal screens in PV cells isolation inside the hybrid photovoltaic-thermal channel on a rooftop designed for natural ventilation in bioclimatic buildings," *International Journal of Scientific and Technology Research*, vol. 7, no. 8, pp. 112–121, 2018.

[10] G. Aspetakis and Q. Wang, "Critical review of Air-Based PVT technology and its integration to building energy systems," Feb. 01, 2025, *KeAi Communications Co.* doi: 10.1016/j.enbenv.2023.10.001.

[11] A. Neugebauer, K. Chen, A. Tang, A. Allgeier, L. R. Glicksman, and L. J. Gibson, "Thermal conductivity and characterization of compacted, granular silica aerogel," *Energy Build*, vol. 79, pp. 47–57, 2014, doi: 10.1016/j.enbuild.2014.04.025.

[12] J. Antonanzas, A. del Amo, A. Martinez-Gracia, A. A. Bayod-Rujula, and F. Antonanzas-Torres, "Towards the optimization of convective losses in photovoltaic-thermal panels," *Solar Energy*, vol. 116, pp. 323–336, 2015, doi: 10.1016/j.solener.2015.04.013.

[13] K. Irshad, K. Habib, and N. Thirumalaiswamy, "Performance evaluation of PV-Trombe wall for sustainable building development," in *Procedia CIRP*, Elsevier B.V., 2015, pp. 624–629. doi: 10.1016/j.procir.2014.07.116.

[14] O. K. Ahmed, K. I. Hamada, A. M. Salih, and R. W. Daoud, "A state of the art review of PV-Trombe wall system: Design and applications," *Environ Prog Sustain Energy*, vol. 39, no. 3, May 2020, doi: 10.1002/ep.13370.

[15] M. M. Awad *et al.*, "Photovoltaic Thermal Collectors Integrated with Phase Change Materials: A Comprehensive Analysis," Feb. 01, 2022, *MDPI*. doi: 10.3390/electronics11030337.

[16] T. Jian, N. Hao, P. Run-Ling, W. Ning, and Z. Lei, "A review on energy conversion using hybrid photovoltaic and thermoelectric systems," *J Power Sources*, vol. 562, Apr. 2023.

[17] T. Ma, H. Yang, Y. Zhang, L. Lu, and X. Wang, "Using phase change materials in photovoltaic systems for thermal regulation and electrical efficiency improvement: A review and outlook," 2015, *Elsevier Ltd.* doi: 10.1016/j.rser.2014.12.003.

[18] X. Yang, L. Sun, Y. Yuan, X. Zhao, and X. Cao, "Experimental investigation on performance comparison of PV/T-PCM system and PV/T system," *Renew Energy*, vol. 119, pp. 152–159, Apr. 2018, doi: 10.1016/j.renene.2017.11.094.

[19] G. Gan and Y. Xiang, "Experimental investigation of a photovoltaic thermal collector with energy storage for power generation, building heating and natural ventilation," *Renew Energy*, vol. 150, pp. 12–22, May 2020, doi: 10.1016/j.renene.2019.12.112.

[20] C. Luo, W. Zou, D. Sun, L. Xu, J. Ji, and M. Liao, "Experimental Study of Thermal Effect of Lacquer Coating for PV-Trombe Wall System Combined with Phase Change Material in Summer," *International Journal of Photoenergy*, vol. 2019, 2019, doi: 10.1155/2019/7918782.

[21] J. Čurpek and M. Čekon, "Climate response of a BiPV façade system enhanced with latent PCM-based thermal energy storage," *Renew Energy*, vol. 152, pp. 368–384, Jun. 2020, doi: 10.1016/j.renene.2020.01.070.

[22] A. S. Abdelrazik, F. A. Al-Sulaiman, and R. Saidur, "Numerical investigation of the effects of the nano-enhanced phase change materials on the thermal and electrical performance of hybrid PV/thermal systems," *Energy Convers Manag*, vol. 205, Feb. 2020, doi: 10.1016/j.enconman.2019.112449.

[23] F. Carlucci, A. Cannavale, A. A. Triggiano, A. Squicciarini, and F. Fiorito, "Phase change material integration in building envelopes in different building types and climates: Modeling the benefits of active and passive strategies," *Applied Sciences (Switzerland)*, vol. 11, no. 10, May 2021, doi: 10.3390/app11104680.

[24] S. Preet, "Water and phase change material based photovoltaic thermal management systems: A review," 2018, *Elsevier Ltd.* doi: 10.1016/j.rser.2017.09.021.

[25] M. Carmona, A. Palacio Bastos, and J. D. García, "Experimental evaluation of a hybrid photovoltaic and thermal solar energy collector with integrated phase change material (PVT-PCM) in comparison with a traditional photovoltaic (PV) module," *Renew Energy*, vol. 172, pp. 680–696, Jul. 2021, doi: 10.1016/j.renene.2021.03.022.

[26] L. A. Hariam, I. Adnan, and O. A. Banw, "Energy and exergy analysis of a novel collector design in a photovoltaic thermal system: An experimental study," *Appl Therm Eng*, vol. 256, Nov. 2024.

[27] W. Lin, Z. Ma, P. Cooper, M. I. Sohel, and L. Yang, "Thermal performance investigation and optimization of buildings with integrated phase change materials and solar photovoltaic thermal collectors," *Energy Build*, vol. 116, pp. 562–573, Mar. 2016, doi: 10.1016/j.enbuild.2016.01.041.

[28] N. Lolli and I. Andresen, "Aerogel vs. argon insulation in windows: A greenhouse gas emissions analysis," *Build Environ*, vol. 101, pp. 64–76, May 2016, doi: 10.1016/j.buildenv.2016.03.001.

[29] T. Ma, J. Zhao, and Z. Li, "Mathematical modelling and sensitivity analysis of solar photovoltaic panel integrated with phase change material," *Appl Energy*, vol. 228, pp. 1147–1158, Oct. 2018, doi: 10.1016/j.apenergy.2018.06.145.

[30] P. C and G. C, *Conductivité thermique des matériaux*. Paris, 2000.

Edelweiss Applied Science and Technology
ISSN: 2576-8484
Vol. 8, No. 6: 2789-2808, 2024
DOI: 10.55214/25768484.v8i6.2558

[31] L. 'Luc, "Law of cooling, heat conduction and Stefan-Boltzmann radiation laws fitted to experimental data for bones irradiated by CO2 laser," *Biomed Opt Express*, vol. 5, no. 3, pp. 701–712, Mar. 2014.

[32] G. 'Mohamed R, A. 'Mohsen, and R. 'Hegazy, "Temperature distribution modeling of PV and cooling water PV/T collectors through thin and thick cooling cross-fined channel box," *Energy Reports*, vol. 8, pp. 1144–1153, 2022.

[33] A. A. Naqvi, A. Ahmed, M. Jamal, A. Majeed, A. Khizar, and B. Shaheer, "Performance Evaluation of Hybrid PVT Air Collector. A Comparative Approach," 2022.

[34] A. Nahar, M. Hasanuzzaman, N. A. Rahim, and S. Parvin, "Numerical investigation on the effect of different parameters in enhancing heat transfer performance of photovoltaic thermal systems," *Renew Energy*, vol. 132, pp. 284–295, Mar. 2019, doi: 10.1016/j.renene.2018.08.008.

[35] J. A. Palyvos, "A survey of wind convection coefficient correlations for building envelope energy systems' modeling," *Appl Therm Eng*, vol. 28, no. 8–9, pp. 801–808, 2008, doi: 10.1016/j.applthermaleng.2007.12.005.

[36] P. L. Woodfield, M. Monde, and Y. Mitsutake, "Measurement of Averaged Heat Transfer Coefficients in High-Pressure Vessel during Charging with Hydrogen, Nitrogen or Argon Gas," *Journal of Thermal Science and Technology*, vol. 2, no. 2, pp. 180–191, 2007, doi: 10.1299/jtst.2.180.

[37] L. C. Woods, "A Note on the Numerical Solution of Fourth Order Differential Equations," *Aeronautical Quarterly*, vol. 5, no. 4, pp. 176–184, 1954, doi: 10.1017/s0001925900001177.

[38] H. Noureddine, A. Vasilios, and Z. M. Tsun, "Resolving The Controversy Over Tin And Gallium Melting In A Rectangular Cavity Heated From The Side," *Numerical Heat Transfer, Part B: Fundamentals*, vol. 44, no. 3, pp. 253–276, 2003, doi: 10.1080/713836378.

[39] Akshayveer, A. P. Singh, A. Kumar, and O. P. Singh, "Effect of natural convection and thermal storage system on the electrical and thermal performance of a hybrid PV-T/PCM systems," in *Materials Today: Proceedings*, Elsevier Ltd, 2019, pp. 1899–1904. doi: 10.1016/j.matpr.2020.08.010.

[40] S. Moench and R. Dittrich, "Influence of Natural Convection and Volume Change on Numerical Simulation of Phase Change Materials for Latent Heat Storage," *Energies (Basel)*, vol. 15, no. 8, Apr. 2022, doi: 10.3390/en15082746.

[41] T. F. Ozueh, J. A. Ajienka, and O. F. Joel, "Exo-Economic Analysis on the Liquefaction Unit of a Baseload LNG Plant," *International Journal of Advances in Engineering and Management (IJAEM)*, vol. 4, p. 1646, 2022, doi: 10.35629/5252-0407164616652.

Edelweiss Applied Science and Technology
ISSN: 2576-8484
Vol. 8, No. 6: 2789-2808, 2024
DOI: 10.55214/25768484.v8i6.2558